Biochimica et Biophysica Acta 1853 (2015) 308–316

Contents lists available at ScienceDirect

Biochimica et Biophysica Acta

journal homepage: www.elsevier.com/locate/bbamcr

Apoptotic human neutrophil peptide-1 anti-tumor activity revealed by cellular biomechanics

Diana Gaspar [1], João M. Freire [1], Teresa R. Pacheco, João T. Barata, Miguel A.R.B. Castanho *

Instituto de Medicina Molecular, Faculdade de Medicina, Universidade de Lisboa, Av. Prof. Egas Moniz, Lisbon 1649-028, Portugal

ARTICLE INFO

Article history:
Received 30 July 2014
Received in revised form 17 October 2014
Accepted 4 November 2014
Available online 13 November 2014

Keywords:
Anticancer peptide
Solid tumor
Membrane charge
Apoptosis
Nanomechanical properties
Atomic force microscopy

ABSTRACT

Cancer remains a major cause of morbidity and mortality worldwide. Although progress has been made regarding chemotherapeutic agents, new therapies that combine increased selectivity and efficacy with low resistance are still needed. In the search for new anticancer agents, therapies based on biologically active peptides, in particular, antimicrobial peptides (AMPs), have attracted attention for their decreased resistance development and low cytotoxicity. Many AMPs have proved to be tumoricidal agents against human cancer cells, but their mode of action is still controversial. The existence of common properties shared by the membranes of bacteria and tumor cells points to similar lipid-targeting mechanisms in both cases. On the other hand, anticancer peptides (ACPs) also induce apoptosis and inhibit angiogenesis. Human neutrophil peptide-1 (HNP-1) is an endogenous AMP that has been implicated in different cellular phenomena such as tumor proliferation. The presence of HNP-1 in the serum/plasma of oncologic patients turns this peptide into a potential tumor biomarker. The present work reveals the different effects of HNP-1 on the biophysical and nanomechanical properties of solid and hematological tumor cells. Studies on cellular morphology, cellular stiffness, and membrane ultrastructure and charge using atomic force microscopy (AFM) and zeta potential measurements show a preferential binding of HNP-1 to solid tumor cells from human prostate adenocarcinoma when compared to human leukemia cells. AFM also reveals induction of apoptosis with cellular membrane defects at very low peptide concentrations. Understanding ACPs mode(s) of action will certainly open innovative pathways for drug development in cancer treatment.

1. Introduction

As cancer remains a significant cause of morbidity and mortality worldwide [1], it is important to rationally analyze the efficacy of conventional therapies and assess its impact on patient's survival and quality of life [1,2]. One of the inspirational sources for anticancer drug leads is the group of so-called antimicrobial peptides (AMPs) [3,4]. In addition to antimicrobial activity, these natural molecules act as conserved effectors in innate immunity [4,5]. Interestingly, many AMPs have proven anticancer activity against human cancer cells [6–9]. The modes of action of these molecules have been extensively studied [10–14], and they have attracted attention since they combine decreased resistance development with low cytotoxicity. AMPs act mainly on the cell membranes via a non-receptor-mediated pathway; therefore, it is difficult for cancer cells to develop resistance [15], which makes AMPs with anticancer activity desirable molecules to be developed as new chemotherapeutic drugs. In addition to membranolytic action, it has been proposed that anticancer peptides (ACPs) trigger intracellular mechanisms of toxicity in tumors [7,16]. Like AMPs, many ACPs have the ability to translocate cell membranes [17] and reach intracellular targets. The activity and selective cancer cell targeting ability of ACPs rely greatly on the increased negative membrane net charge as well as on differences of membrane fluidity presented by tumor cells when compared to normal tissues [15,18].

Defensins are a group of cationic AMPs that have been isolated from different species [19], being the α- and β-defensins from human origin the most intensively studied [20]. α-Defensins are the human neutrophil peptides, or HNPs, which are major components of the azurophilic granules of neutrophils [21,22] in which concentrations of ~10 mg/ml can be achieved [23]. These 30 amino acid residue peptides are produced and released in response to microbial invasions, rapidly inactivating a large spectrum of potential pathogens, either Gram-positive or Gram-negative bacteria, and yeasts [24]. Their effect in cell division, attraction, and differentiation of immune cells and wound healing has been also described [25]. Importantly, the human neutrophil peptide-1, HNP-1, as for other AMPs, showed simultaneous antimicrobial and anticancer

Abbreviations: AMPs, antimicrobial peptides; ACPs, anticancer peptides; HNP-1, human neutrophil peptide-1; EthD-1, ethidium homodimer-1; R_{ms}, root-mean-square roughness; HNPs, human neutrophil peptides; PS, phosphatidylserine; GAGs, glycosaminoglycans

* Corresponding author. Tel.: +351 217985136; fax: +351 217999477.
E-mail addresses: dianagaspar@fm.ul.pt (D. Gaspar), joaofreire@fm.ul.pt (J.M. Freire), tr.pacheco@fm.ul.pt (T.R. Pacheco), joao_barata@fm.ul.pt (J.T. Barata), macastanho@fm.ul.pt (M.A.R.B. Castanho).

[1] The authors contributed equally to this work.

http://dx.doi.org/10.1016/j.bbamcr.2014.11.006
0167-4889/

activity [26,27]. In addition, HNP-1 has been suggested as a potential prognostic biomarker in cancer [28–34] since it has been detected in epithelial tumors and is associated with tumor necrosis when expressed intratumorally [35,36]. Up-regulated in cancers such as bladder, gastric, and colorectal [29,33,34], the role of HNP-1 on the tumor microenvironment and directly on the cancer cell is still unclear. Although it is known that the HNP-1 damages cell membranes and enters cells [37], the exact mechanism of cell death has remained elusive for more than 20 years.

In this work, we show the effects of HNP-1 on human prostate adenocarcinoma (PC-3) and human acute lymphoblastic leukemia (MOLT-4) cells using spectroscopic techniques and atomic force microscopy (AFM). AFM techniques resolve the cellular ultrastructure at the nanometer scale [38]. In oncology, AFM has been used to reveal details of the cell membrane structure and morphology [39–41], interaction with different molecules [42], and elasticity [40,41,43]. In the present study, results on cellular morphology, stiffness, and biomembrane biophysical properties such as surface density charge and roughness allowed the identification of the cellular structures that are damaged by HNP-1. These damages interfere with cells' ability to migrate and invade different organs after interacting with HNP-1.

2. Materials and methods

2.1. Biological material and reagents

Human neutrophil peptide-1 (HNP-1; Ala-Cys-Tyr-Cys-Arg-Ile-Pro-Ala-Cys-Ile-Ala-Gly-Glu-Arg-Arg-Tyr-Gly-Thr-Cys-Ile-Tyr-Gln-Gly-Arg-Leu-Trp-Ala-Phe-Cys-Cys: Cys^2-Cys^{30}, Cys^4-Cys^{19}, Cys^9-Cys^{29}) was purchased from Bachem. Adherent cancer cell line PC-3 (human prostate adenocarcinoma) and suspension cell line MOLT-4 (human acute lymphoblastic leukemia) were purchased from American Type Culture Collection (ATCC, CRL-1435, and CRL-1582, respectively). RPMI-1640 media, heat-inactivated fetal bovine serum (FBS), penicillin and streptomycin solution, 200 mM glutamine solution, and trypsin EDTA were obtained from Life Technologies. Glutaraldehyde was from Sigma.

2.2. Cell culture

Adherent cancer cell line PC-3 was cultured as a monolayer in RPMI-1640 media supplemented with 10% FBS, 2 mM glutamine, 100 U/ml penicillin, and 100 U/ml streptomycin and maintained at 37 °C and 5% CO_2 in a humidified environment. MOLT-4 cell line was cultured in suspension in RPMI-1640 media supplemented with 10% FBS and 2 mM glutamine and also maintained at 37 °C and 5% CO_2 in a humidified environment.

2.3. Cell live/dead assay using flow cytometry techniques

The cytotoxicity of HNP-1 against PC-3 and MOLT-4 cells was evaluated using a LIVE/DEAD® Viability/Cytotoxicity Assay Kit (L-3224) obtained from Life Technologies. This kit is based on the use of two fluorescent probes, calcein AM, and Ethidium homodimer-1 (EthD-1) that are sensitive to intracellular enzymatic activity and plasma membrane integrity, respectively. The use of these probes allows discriminating between live and dead cells after interaction with HNP-1. Live cells display green and dead cells red fluorescence, respectively. Calcein AM is a cell permeable probe, which is converted by intracellular esterase activity, ubiquitous in live mammalian cells, to green fluorescent (530 nm) calcein. Dead cells are stained by EthD-1 dye, which binds to cellular DNA of cells with their membrane compromised/permeabilized. Double staining also occurs in dead cells, indicating that some esterase activity remained prior to cell damage and further cell death [44]. Confluent PC-3 cells were washed with phosphate buffer saline (PBS) after trypsinization, while MOLT-4 cells were directly washed with PBS. Cells were counted with a cell counter (Scepter 2.0 from Milipore), diluted to 7×10^5 cell/ml and incubated for 4 h at 37 °C with increasing concentrations of peptide up to 10 μM, previously dissolved in PBS buffer. This incubation was performed in culture medium supplemented without serum. Cells were then washed and suspended in PBS buffer. Cell labeling with calcein AM and EthD-1 was performed according to the manufacturer's instructions. Briefly, 2 μL/ml of calcein AM and 4 μL/ml of EthD-1 stock solution were added to each sample and incubated 20 min at room temperature protected from light before measurement. Samples were loaded into a 96-well microplate, and each well was acquired using a BD LSR Fortessa cell analyzer equipped with a high throughput screening (HTS) module and a 488 nm laser. Each measurement consisted in collecting and recording the events of 180 μL of each sample. Calcein green fluorescence and EthD-1 red fluorescence emission were recorded using 530/30 and 610/20 band-pass filters, respectively. Live and dead control populations were also measured for proper live and dead populations discrimination and gating. Dead cells were obtained by inducing cell death with 70% isopropanol solution. Forward and side scatter data were also collected to evaluate cell damage and morphology changes induced by HNP-1. The percentage of HNP-1-induced cell death/damage was calculated according to control cell population gating and manufacturer's instructions. The peptide concentration required to kill half of the cancer cells (IC_{50}) was calculated by fitting a sigmoidal dose–response function [45] to cell death percentage data as a function of HNP-1 concentration using GraphPad Prism v6.0 analysis software.

Each sample was collected in triplicate and in two different days using independent cellular suspensions.

2.4. Zeta potential measurements of live PC-3 and MOLT-4 cells in the presence of HNP-1

The surface charge density of the cancer cells and the electrostatic attraction of HNP-1 toward them were evaluated using zeta-potential technique. Charged particles that are suspended in solution attract ions with opposite charge to their surface. These ions cover the particle surface and bound to it very strongly, forming the Stern layer. In addition to this layer, a second one is formed where the ions diffuse more freely. When the particle diffuses through the solution, the strongly bound ions move with it, contrary to the ions located in the diffuse boundary. The zeta-potential is the potential that exists at this boundary and can be determined by the electrophoretic mobility of the particles in solution [46]. For these experiments, confluent PC-3 cells were washed with PBS buffer after trypsinization. Cells were diluted to 1×10^5 cells/ml in PBS buffer. MOLT-4 cells were washed with PBS buffer, counted and diluted to 2.5×10^5 cells/ml in PBS buffer. Cellular suspensions with and without HNP-1 (0–10 μM) were dispensed into disposable zeta cells with gold electrodes and allowed to equilibrate for 30 min at 37 °C. A set of 15 measurements (~40 runs each) were performed with a constant voltage of 40 V. Control values were obtained by measuring the surface charge of each cellular suspension in the absence of HNP-1 (0 μM). The complete experiment was carried out at least two times using independent cellular suspensions.

2.5. Atomic force microscopy imaging

AFM images were acquired using a JPK Nano Wizard II (Berlin, Germany) mounted on a Zeiss Axiovert 200 inverted microscope (Göttingen, Germany). The AFM head is equipped with a 15-μm z-range linearized piezoelectric scanner and an infrared laser. PC-3 cells were culture in monolayer on IbiTreat 35 mm μ-dishes from Ibidi at 5×10^4 cell/ml for 2 days. For control images, the culture medium was replaced with new medium supplemented without serum followed by an incubation of 4 h. Since we were interested in observing in detail the membrane structure, we proceeded to cell fixation with glutaraldehyde before imaging. After culture media removal, cells were washed with PBS buffer and then fixed for 10 min at room temperature in 2% glutaraldehyde solution, washed with PBS and sterile mili-Q water,

and finally air-dried. For studying the morphological changes that cells endure in HNP-1 presence, cells grown for 2 days on the IbiTreat μ-dishes were added of new culture medium supplemented without serum and with 5 μM HNP-1 final concentration. Cells and peptide were incubated for 4 h and then washed and fixed using the same procedure for control samples. Measurements were carried out in air and in intermittent contact mode using uncoated silicon ACL cantilevers from Applied NanoStructure (Santa Clara, CA, USA). ACL cantilevers had typical resonance frequencies between 145 and 230 kHz and an average spring constant of 45 N/m. Cells were first visualized through the optical microscope before being selected for imaging. Due to irregular cellular size and shape, total scan areas with 70 × 70 to 75 × 75 μm were imaged with a resolution of 512 × 512 pixels and scan speeds lower than 1 Hz. Height and error images were recorded and images were line fitted as required. The height profile of 10 treated and 12 untreated cells, was acquired through a cross section of each cell using the JPK SPM Data Processing version 4.2.61. The surface roughness of control and HNP-1-treated PC-3 cells was defined as the root-mean-square roughness (R_{ms}) calculated from AFM height images and using Gwyddion software version 2.33 [47]. R_{ms} values were obtained from the whole cell but also from different areas, namely, nucleus and cytoplasm. Squared areas of 2.5 × 2.5 μm were selected and assigned as nuclear, cytoplasmic, or cell boundaries and finally analyzed. The R_{ms} median of each group of squares corresponds to the final R_{ms} value of the cellular component (nuclei and cytoplasm). R_{ms} of the whole cell was calculated as the median of all squares analyzed (nuclei, cytoplasm, and cell boundaries). Cells were observed and imaged throughout three different days in different passages using independent grown cultures.

2.6. Young's modulus (E) of prostate tumor cells determination

All studies were conducted using a JPK Nano Wizard II (Berlin, Germany) mounted on a Zeiss Axiovert 200 inverted microscope (Göttingen, Germany). The combination AFM-optical microscope allows the lateral positioning of the AFM tip over the cell body with micrometer precision. Elasticity measurements were performed on live cells cultured as described previously for AFM imaging (control and HNP-1-treated samples). The culture medium was removed and the cells washed and kept in PBS buffer at room temperature. Data collection was carried out until 1 h after initializing the measurements for ensuring the healthiness of the cells. After that, a new μ-dish was observed. Triangular-shaped silicon nitride cantilevers (OMCL-TR400PSA-1, Olympus) were used for indenting the center of PC-3 cells, typically

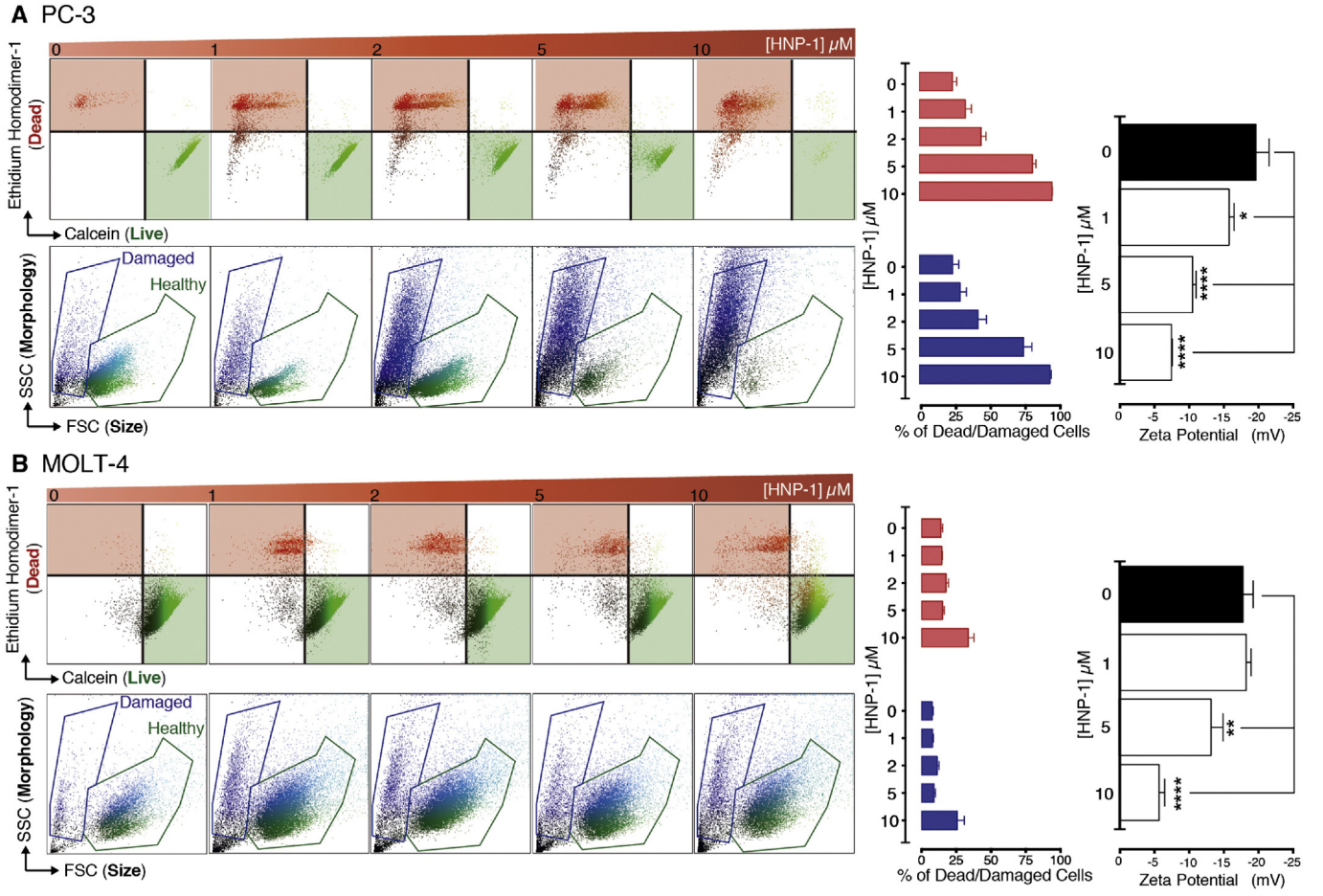

Fig. 1. Effects of human neutrophil peptide-1 (HNP-1) on tumor cell viability and surface charge density of solid and hematological tumor cells. Human prostate adenocarcinoma cells (PC-3, A) and human acute lymphoblastic leukemia cells (MOLT-4, B) were incubated with HNP-1 up to a maximum concentration of 10 μM for 4 h. The killing activity of HNP-1 was determined by flow cytometry using a LIVE/DEAD assay kit (*upper correlogram*) using calcein (green) and ethidium homodimer-1 (red) fluorescent dyes to detect live and dead cells, respectively. HNP-1-induced changes in cell morphology (*lower correlogram*) were used to follow cellular alterations (blue). Live and dead control populations were used for proper live and dead population gate discrimination (green and red, respectively). The percentage of HNP-1-induced cell death/damage was calculated according to population gating frequency over total cell population. Alterations in cell membrane charge density in the presence of HNP-1 were followed by zeta potential measurements. All experiments were repeated in different days using independently grown cell cultures. *0.01 < *p*-value < 0.05; **0.001 < *p*-value < 0.01; ***0.0001 < *p*-value < 0.001; ****p*-value < 0.0001.

corresponding to the nuclear area. Cantilever spring constants (typically 0.02 N/m) were calibrated by the thermal noise fluctuations method [48] before and after use and no change between the values was detected. Force curves (three per cell) were obtained at a maximum applied force of 400 pN, sufficient to allow a good signal-to-noise ratio without damaging the cells. The Hertz model was fitted to the approach curves for extracting the Young's modulus (E). The measurement point was selected in order to reduce the lateral heterogeneity of the mechanical response that is expected from live cells. The procedure was repeated in at least three different days using independently grown cultures in different passages in a total of 59 untreated and 30 treated cells.

2.7. Statistical analysis

Quantitative data were processed with Excel 2007 (Microsoft, USA) and GraphPad Prism 6 software. Means and standard deviations are shown in the figures. Pairwise significances were calculated using one-way ANOVA and two-tailed unpaired t-test. For R_{ms} values, an unpaired two-tailed nonparametric Mann–Whitney test was used. The p-values lower than 0.05 were considered significant.

3. Results and discussion

Prostate carcinoma is the third leading cause of oncologic deaths following lung and colorectal cancers and has the highest incidence rate among all cancers in men [49]. For prostate cancer treatment, options are currently hormone therapy, surgery, or irradiation [50,51]. Despite the available therapeutic arsenal, prostate cancer cells do not respond well to single or multiple drug regimens [52,53] and side effects are very significant. New peptide-based drugs might be an alternative [8,9,54]. For hematological malignancies, similar obstacles in treatment have been described due to the existence of multiple cell types with variable genotype/karyotype [55], which limits the benefits of conventional therapies for leukemia eradication.

3.1. HNP-1 cytotoxic activity and correlation with cell membrane surface charge

The HNP-1 cytotoxic activity against tumor cells was tested using a live/dead viability/cytotoxicity assay kit. Fig. 1 shows the progression of cell death and cell damage in response to HNP-1 concentration in PC-3 and MOLT-4 cells. The concentrations of HNP-1 that are detected in multiple clinical situations in moderate clinical states, severe infections, or tumor patients are variable [29,32,33,56]. Table S1 on Supplementary Data gathers information from studies performed with HNPs in normal and tumor cells, including the analysis of their heterogeneous impact on cell viability and proliferation. In the viability experiments we performed, the concentration range tested was below the values observed in severe infections [56] and within the range of the mitogenic values of HNP-1 for cancers such as renal cell carcinoma [33]. Our results show that HNP-1 is highly cytotoxic to PC-3 cells, in contrast with the MOLT-4 cell line (Fig. 1). For PC-3 cells, an IC_{50} of 2.2 ± 0.3 μM was obtained within the range of HNP-1 concentrations tested. At 10 μM, more than 90% of PC-3 cells were dead, while for MOLT-4 cells the same peptide concentration affected less than 30% of the cell population. Side scatter flow cytometry analysis showed an increase in granularity concomitant with membrane permeabilization and cell death, which raises the hypothesis that the peptide has a powerful effect on PC-3 cell morphology. A much lower degree of granularity was observed on MOLT-4 cells in parallel to the lower toxicity values. It is reasonable to speculate that HNP-1 anticancer action comprises an initial step of cell membrane permeabilization followed by increased granularity due to apoptosis initiation. Mitochondria and nuclei perturbation together with the formation of apoptotic vesicles and chromatin condensation are responsible for the increase in the granularity in this phase.

Cancer cell membranes are more anionic at their surface than normal cells [7,20] because of the presence of the phosphatidylserine (PS) phospholipid and negatively charged macromolecules such as glycosaminoglycans (GAGs) on the outer leaflet of the membrane [20,57]. The zeta potential reflects the electrostatic potential at the shear plane of a scattering particle or cell, which in turn depends on charge density

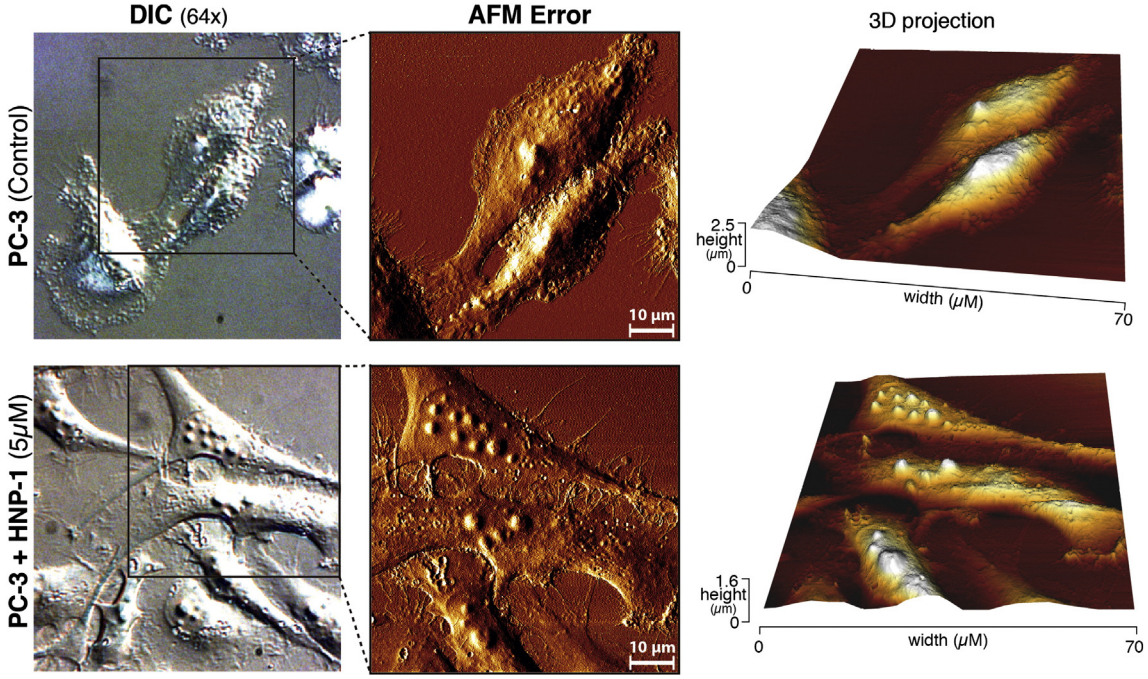

Fig. 2. Morphological examination of tumor cells using atomic force microscopy (AFM). Differential interference contrast (DIC) images, AFM error images, and three-dimensional (3D) projections of human prostate adenocarcinoma (PC-3) cells in the absence and presence of human neutrophil peptide-1 (HNP-1) are shown. Control cells show a typical epithelial morphology that is compromised after incubation with HNP-1.

[46,58]. This parameter has been used not only for describing the surface electrostatics of cells in different environmental states [59] but also for assessing cellular phenomena such as adhesion and interaction with peptides [10,60–63]. Therefore, we next evaluated the zeta potential of live PC-3 and MOLT-4 cells in the presence of increasing concentrations of HNP-1. Adding HNP-1 to PC-3 and MOLT-4 cells increased the zeta potential from -19.6 ± 1.9 mV to -17.8 ± 1.5 mV, respectively, toward neutralization (Fig. 1), which shows that the peptide

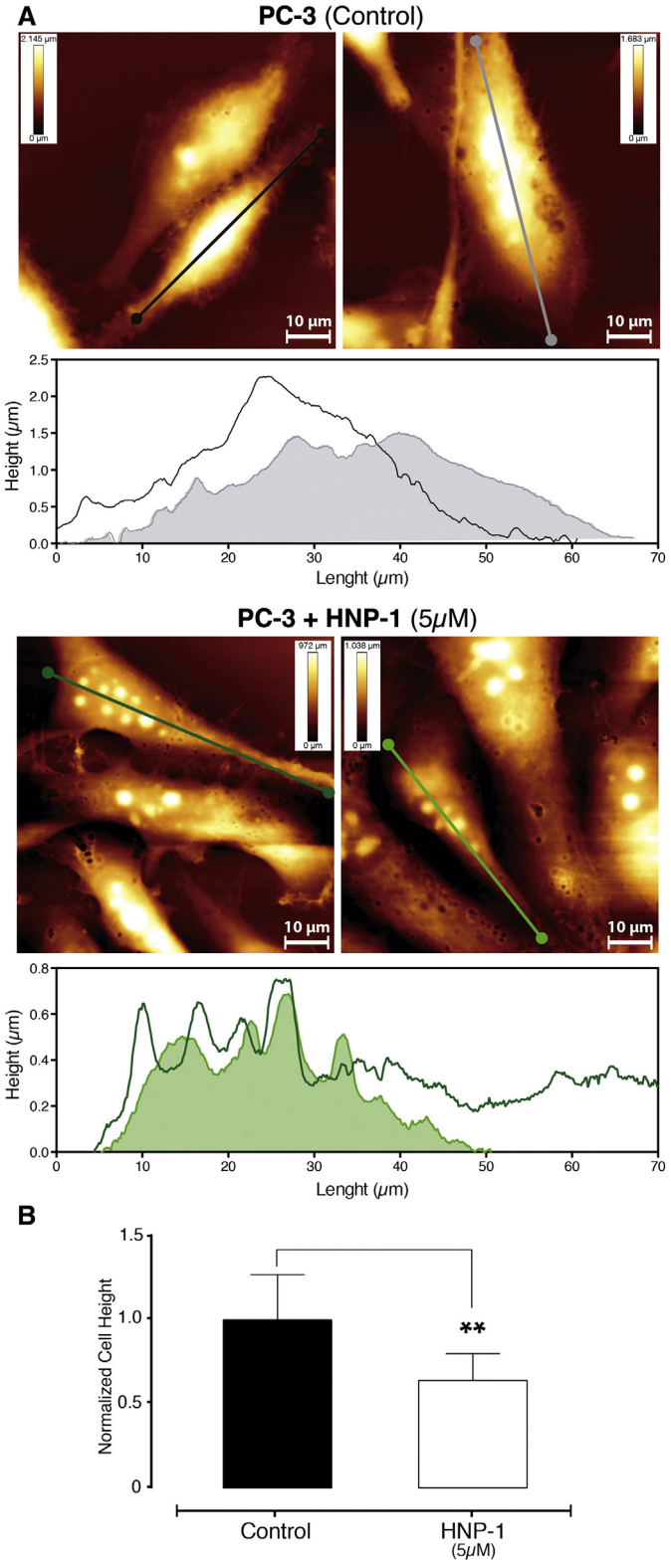

Fig. 3. Tumor cell topography revealed by atomic force microscopy (AFM). Representative AFM height images and cell height profiles of human prostate adenocarcinoma (PC-3) cells in the absence and presence of human neutrophil peptide-1 (HNP-1) are represented in A. Height profiles reveal that in the presence of HNP-1, cells appear flattened with nuclear fragmentation. Cell height normalized to control from 12 control cells and 10 HNP-1-treated cells are shown in panel B. There is a statistically significant difference between both cell groups. A two-tailed unpaired *t*-test was employed. $^{**}0.001 < p\text{-value} < 0.01$.

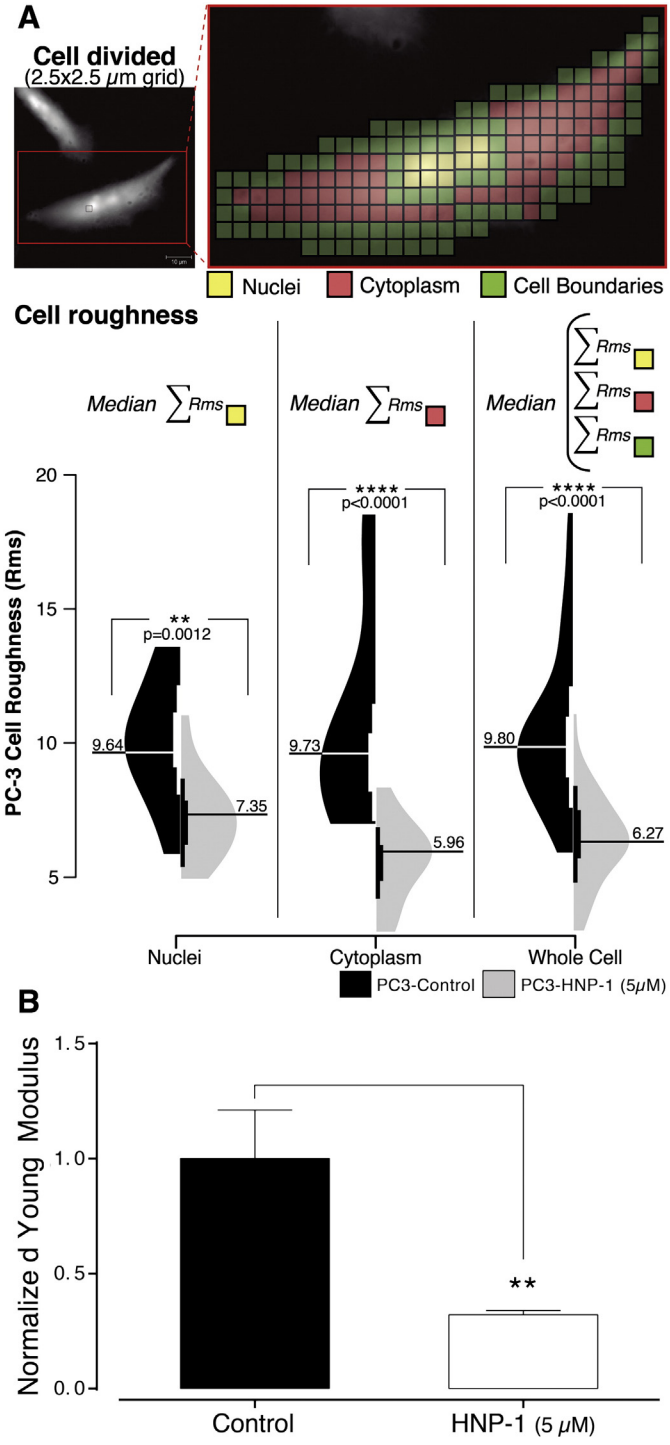

Fig. 4. Cell membrane roughness and elasticity evaluation of human prostate cancer cells. (A) Human prostate adenocarcinoma (PC-3) cell roughness, R_{ms}, was evaluated on the nuclear and cytoplasm areas as well as over the entire cell from AFM height images. The cell was divided into a 2.5 × 2.5 μm grid and each one assigned as nuclear (yellow), cytoplasmic (red), or cell (green). The R_{ms} median of each group of squares corresponds to the final R_{ms} value of the cellular component (nuclei and cytoplasm). R_{ms} of the whole cell was calculated as the median of all squares analyzed (nuclei, cytoplasm, and cell boundaries). The absolute R_{ms} values decrease after peptide treatment revealing perturbations of the cell membrane. Eleven control cells (black) were compared to 16 HNP-1-treated cells (grey). (B) Cells' elasticity was determined by the normalized Young's modulus (E) calculation after indenting live cells. HNP-1 caused a decrease in E, thus an increase in cell elasticity which reflects changes associated to cytoskeleton organization and nuclear integrity. A total of 59 control cells and 30 HNP-1-treated cells over at least three independent days were measured and analyzed. A two-tailed unpaired t-test was employed. *0.01 < p-value < 0.05; **0.001 < p-value < 0.01; ***0.0001 < p-value < 0.001; ****p-value < 0.0001.

binds to both types of cells. The differences in the surface charge of both cell types may reflect different membrane compositions, which ultimately can account for differences in cell behavior in the presence of the peptide [64,65]. Indeed, the differential distribution of membrane components contributing to the net anionic character of the cellular surface, such as PS and charged gangliosides, has been identified as key-factors for the efficacy and selectivity of biologically active peptides [64,66]. It should be also stressed that similarly to what we have reported before for a customized ACP [16] and contrary to what has been described for AMPs [10], killing preceded full neutralization of the cell's surface potential for both malignant cells (Fig. 1). Thus, cell death is not directly related to complete membrane charge neutralization.

3.2. AFM imaging of human prostate cancer cells

Using AFM, we observed the direct membrane damage of HNP-1 on human prostate cancer (Fig. 2) and MOLT-4 cells (Supplementary Data). Fig. 2 shows representative height AFM images at 5 μM HNP-1, above the IC_{50}. Under normal culture conditions, the PC-3 cells present an epithelial morphology with variable dimensions, with a relatively smooth and intact surface and with pseudopodia. The cell nucleus is distinctively visible and appears as a raised area in white in each image. After HNP-1 addition, cells suffered a variety of morphological modifications. The cell shape became irregular and the fragmentation of the nucleus was visible (Fig. 2). Cells also appeared collapsed. Height profiles of the cells were drawn using JPK software (Fig. 3). The observed cells' height decrease caused by HNP-1 treatment (Fig. 3B) reflects important changes on the cells' cytoskeleton structure after the peptide interaction with the cell membrane and its entrance into the cell. Previous studies using K562 and Raji cells have shown that even though defensins permeabilize plasma membranes, this perturbation might not be sufficient to induce significant cytolysis [67]. Induction of DNA strand breaks occurs and is likely to participate in the cell death caused by HNPs [67]. It was thus proposed that at least two mechanisms of cell injury occur, first, a membrane attack and, second, a major DNA injury (after 4–6 h of peptide incubation). A different study also showed that HNP-1-induced *Trypanosoma cruzi* cell destruction after early internalization through pores on the cellular and flagellar membranes [68]. There was minimal cellular damage followed by cytoplasm and organelle damage and DNA fragmentation. Our results extend these observations and indicate that DNA injury occurs by chromatin condensation also in solid tumor cells. Interestingly, at the same tested concentration HNP-1 did not induce the collapse of MOLT-4 cells (please refer to online Supplementary Data, Figs. S1 and S2 of this article), which contrasts with previous studies on K562 (chronic myeloid leukemia) and Raji (Burkitt's lymphoma) cells and suggests heterogeneity in the sensitivity to HNP-1, and possibly other ACPs, within hematological cancers. The cell membrane composition might have an important role in this heterogeneity [64,66].

The roughness of the cell membrane is an indicator of the homeostasis of cells because it can be related to different cellular mechanisms such as motility and adhesion [69,70]. Further studies show that roughness helps elucidating the mechanism of cellular death caused by external molecules. For instance, surface roughness has been used to characterize the metal-induced cytotoxic effects on pancreatic cells [71]. We have determined the root-mean-square roughness, R_{ms}, on AFM height images on 4–5 different selected areas (2.5 × 2.5 μm) using Gwyddion 2.33 version software [47]. The results are shown in Fig. 4A and reveal a generalized decrease in the membrane roughness after HNP-1 treatment. Membrane roughness is sensitive to the membrane-skeleton interface structure and integrity [72–74]. Membrane roughness decreases when there is a weaker mechanical support provided by the cell cytoskeleton to the lipid bilayer. This has been observed, for example, in red blood cells in some blood pathologies and after treatment with cytoskeleton-depolymerizing agents [73]. The detachment of the cytoskeleton network from the lipid bilayer results in this decreased support and in a subsequent folding and rearrangement of the lipid bilayer [73].

3.3. Nanoindentation of prostate tumor cells after HNP-1 treatment and Young's modulus (E) determination

Cancer cells provide their own growth signals while ignoring growth inhibitory signals, avoid cell death, replicate without limit, sustain angiogenesis, and invade tissues through basement membranes and capillary walls. As a dynamic system, cancer cells continuously adapt their physical and chemical properties and their deformability. This has implications in many cellular processes such as signaling, cytoadherence, migration, invasion, and metastatic ability [75]. Indeed, for tumor cells to metastasize, it is necessary that epithelial cancer cells penetrate the endothelial layer and this step depends on both cell elasticity and deformability [75]. It has been reported that tumor cells have a low elasticity module and thus are softer than normal cells [39,75–78], and others have proposed that this is related to metastatic potential [79]. There are several techniques available for measuring and assessing mechanical properties of human cells [80–82] having AFM assumed an important position [43,79,83,84]. In these experiments, a local deformation is induced on the cell surface by using a blunt tip on the free end of a cantilever. Force curves are obtained and the deformability or compliance of normal and malignant cells is retrieved from the elastic modulus. This approach has been used before with particular relevance on the work of Plodinec and coworkers. In this particular case, an indentation-type AFM (IT-AFM) was used to reveal the stiffness profile of normal/benign and malignant tissues obtained from breast biopsies [85]. The importance of indentation studies is highlighted in this work, in which mechanobiological markers for tumor development and clinical prognostics were identified [85]. Other applications of force curve analysis include the monitoring of the nanomechanical properties of different biological samples while changing environmental conditions [86–88]. Elasticity values of PC-3 cells were obtained in live cells using a pyramidal-shaped tip and by indenting the cell body. The obtained individual force-displacement curves were converted into force–distance curves (*F–d*), and finally these curves were shifted to remove the offset. Fig. 4B shows the normalized values of *E* obtained for control and HNP-1-treated cells at 5 μM after analyzing the indentation portion of the *F–d* curves and application of the Hertz model with JPK software. The relative change of the elastic modulus is used to monitor the effect of external molecules on the deformability of cells [89]. However, values of *E* for mammalian cells have a great variability [90]. The mechanical behavior of the cell surface includes typically elastic and viscous components [91]. As cytoskeleton components are known to be heterogeneous in their elastic moduli, dimensions, and also distribution [92], variable cell stiffness and consequently variable *E* values are to be expected. In this study, *E* values reflect mainly local mechanical information. Several parameters were controlled to reduce data variability. Local elasticity information was collected with controlled force, velocity, and indentation depth so the contribution of viscous component as well as the contribution of cell structures underneath the membrane could be minimized. Three curves were collected from each analyzed cell and no significant changes were observed between them. Fig. S3 on the online Supplementary data represents typical force curves. Our results show that HNP-1-treated cells have a lower *E*, revealing a change in their mechanical properties. This effect is related to internal damage in the cytoskeleton and/or nuclear region and reflects the apoptotic effect of the peptide [70] in agreement with AFM images and zeta potential measurements. These changes in cell's elasticity are expected to hamper both cell motility and ability to deform/spread, therefore influencing subsequent invasion and metastasis to other organs such as bones.

4. Conclusions

In this study, we apply an innovative combination of techniques to study the effects of HNP-1 on cells of solid and hematological tumors. Cytotoxicity experiments and measurements of membrane surface charge of solid and hematological tumor cell lines revealed a preferential activity of HNP-1 toward solid tumors. Differences in the membrane composition of both types of tumors are expected to be behind the peptide's selectivity. In this regard, it is tempting to speculate that the substantial membrane alterations that solid tumor cells must undergo to overcome the physical barriers imposed on epithelial cells, as opposed to the minimal constrains imposed on hematopoietic cells, may render the former more sensitive to the cytotoxic effect of ACPs. Recent studies pinpoint the importance of sialic acid moieties of glycoproteins or gangliosides on the surface of breast cancer cells which represent binding sites for AMPs [93]. The expression of both these molecules and also of

the lipids of the membrane bilayer can be expected to vary between different cancers and between solid and non-solid tumors [94], thus functioning as a trigger for ACPs selectivity and accounting for a strong binding ability for some peptides. Our results are consistent with HNP-1 translocation to the interior of the cell and subsequent nuclear DNA and cytoskeleton damage. The end result is cell collapse due to apoptosis. Overall, we show that cell death occurs without full neutralization of the cancer cell membrane, which distinguishes ACPs' from AMPs' mode of action. Although the identification of the exact cancers where its use may be most effective warrants further investigation, HNP-1 shows great potential as a powerful ACP drug lead.

Acknowledgments

This work was supported by a grant from Laço (Portugal). Diana Gaspar and João Freire acknowledge FCT-MEC for fellowships SFRH/BPD/73500/2010 and SFRH/BD/70423/2010, respectively.

Appendix A. Supplementary data

Supplementary data to this article can be found online at http://dx.doi.org/10.1016/j.bbamcr.2014.11.006.

References

[1] S. Al-Benna, Y. Shai, F. Jacobsen, L. Steinstraesser, Oncolytic activities of host defense peptides, Int. J. Mol. Sci. 12 (2011) 8027–8051.
[2] F. Harris, S.R. Dennison, J. Singh, D.A. Phoenix, On the selectivity and efficacy of defense peptides with respect to cancer cells, Med. Res. Rev. 33 (2013) 190–234.
[3] D. Gaspar, A.S. Veiga, M.R.B. Castanho, From antimicrobial to anticancer peptides. A review, Front. Microbiol. 4 (294) (2013) 1–16.
[4] K.C. Mulder, L.A. Lima, V.J. Miranda, S.C. Dias, O.L. Franco, Current scenario of peptide-based drugs: the key roles of cationic antitumor and antiviral peptides, Front. Microbiol. 4 (321) (2013) 1–23.
[5] R.E.W. Hancock, H.G. Sahl, Antimicrobial and host-defense peptides as new anti-infective therapeutic strategies, Nat. Biotechnol. 24 (2006) 1551–1557.
[6] G. Berge, L.T. Eliassen, K.A. Camilio, K. Bartnes, B. Sveinbjornsson, O. Rekdal, Therapeutic vaccination against a murine lymphoma by intratumoral injection of a cationic anticancer peptide, Cancer Immunol. Immunother. 59 (2010) 1285–1294.
[7] J.S. Mader, D.W. Hoskin, Cationic antimicrobial peptides as novel cytotoxic agents for cancer treatment, Expert Opin. Investig. Drugs 15 (2006) 933–946.
[8] H. van Zoggel, G. Carpentier, C. Dos Santos, Y. Hamma-Kourbali, J. Courty, M. Amiche, J. Delbe, Antitumor and angiostatic activities of the antimicrobial peptide dermaseptin B2, PLoS ONE 7 (2012) e44351.
[9] K.R. Wang, B.Z. Zhang, W. Zhang, J.X. Yan, J. Li, R. Wang, Antitumor effects, cell selectivity and structure–activity relationship of a novel antimicrobial peptide polybia-MPI, Peptides 29 (2008) 963–968.
[10] C.S. Alves, M.N. Melo, H.G. Franquelim, R. Ferre, M. Planas, L. Feliu, E. Bardaji, W. Kowalczyk, D. Andreu, N.C. Santos, M.X. Fernandes, M.A. Castanho, Escherichia coli cell surface perturbation and disruption induced by antimicrobial peptides BP100 and pepR, J. Biol. Chem. 285 (2010) 27536–27544.
[11] M.M. Domingues, P.M. Silva, H.G. Franquelim, F.A. Carvalho, M.A. Castanho, N.C. Santos, Antimicrobial protein rBPI-induced surface changes on Gram-negative and Gram-positive bacteria, Nanomedicine 10 (2013) 543–551.
[12] K.A. Brogden, Antimicrobial peptides: pore formers or metabolic inhibitors in bacteria? Nat. Rev. Microbiol. 3 (2005) 238–250.
[13] C.D. Fjell, J.A. Hiss, R.E. Hancock, G. Schneider, Designing antimicrobial peptides: form follows function, Nat. Rev. Drug Discov. 11 (2012) 37–51.
[14] M.N. Melo, R. Ferre, M.A. Castanho, Antimicrobial peptides: linking partition, activity and high membrane-bound concentrations, Nat. Rev. Microbiol. 7 (2009) 245–250.
[15] C. Chen, J. Hu, P. Zeng, F. Pan, M. Yaseen, H. Xu, J.R. Lu, Molecular mechanisms of anticancer action and cell selectivity of short alpha-helical peptides, Biomaterials 35 (2014) 1552–1561.
[16] C. Sinthuvanich, A.S. Veiga, K. Gupta, D. Gaspar, R. Blumenthal, J.P. Schneider, Anticancer beta-hairpin peptides: membrane-induced folding triggers activity, J. Am. Chem. Soc. 134 (2012) 6210–6217.
[17] S.T. Henriques, M.N. Melo, M.A. Castanho, Cell-penetrating peptides and antimicrobial peptides: how different are they? Biochem. J. 399 (2006) 1–7.
[18] F. Schweizer, Cationic amphiphilic peptides with cancer-selective toxicity, Eur. J. Pharmacol. 625 (2009) 190–194.
[19] T. Ganz, Defensins: antimicrobial peptides of innate immunity, Nat. Rev. Immunol. 3 (2003) 710–720.
[20] D.W. Hoskin, A. Ramamoorthy, Studies on anticancer activities of antimicrobial peptides, Biochim. Biophys. Acta 1778 (2008) 357–375.
[21] T. Ganz, R.I. Lehrer, Antimicrobial peptides of vertebrates, Curr. Opin. Immunol. 10 (1998) 41–44.
[22] A.J. Ouellette, M.E. Selsted, Paneth cell defensins: endogenous peptide components of intestinal host defense, FASEB J. 10 (1996) 1280–1289.
[23] H. Tanabe, J. Yuan, M.M. Zaragoza, S. Dandekar, A. Henschen-Edman, M.E. Selsted, A.J. Ouellette, Paneth cell alpha-defensins from rhesus macaque small intestine, Infect. Immun. 72 (2004) 1470–1478.
[24] J. Jarczak, E.M. Kosciuczuk, P. Lisowski, N. Strzalkowska, A. Jozwik, J. Horbanczuk, J. Krzyzewski, L. Zwierzchowski, E. Bagnicka, Defensins: natural component of human innate immunity, Hum. Immunol. 74 (2013) 1069–1079.
[25] J. Winter, M. Wenghoefer, Human defensins: potential tools for clinical applications, Polymers 4 (2012) 691–709.
[26] S.T. McKeown, F.T. Lundy, J. Nelson, D. Lockhart, C.R. Irwin, C.G. Cowan, J.J. Marley, The cytotoxic effects of human neutrophil peptide-1 (HNP1) and lactoferrin on oral squamous cell carcinoma (OSCC) in vitro, Oral Oncol. 42 (2006) 685–690.
[27] M. Nishimura, Y. Abiko, Y. Kurashige, M. Takeshima, M. Yamazaki, K. Kusano, M. Saitoh, K. Nakashima, T. Inoue, T. Kaku, Effect of defensin peptides on eukaryotic cells: primary epithelial cells, fibroblasts and squamous cell carcinoma cell lines, J. Dermatol. Sci. 36 (2004) 87–95.
[28] J. Albrethsen, R. Bogebo, S. Gammeltoft, J. Olsen, B. Winther, H. Raskov, Upregulated expression of human neutrophil peptides 1, 2 and 3 (HNP 1–3) in colon cancer serum and tumours: a biomarker study, BMC Cancer 5 (2005) 8.
[29] J. Albrethsen, C.H. Moller, J. Olsen, H. Raskov, S. Gammeltoft, Human neutrophil peptides 1, 2 and 3 are biochemical markers for metastatic colorectal cancer, Eur. J. Cancer 42 (2006) 3057–3064.
[30] N. Droin, J.B. Hendra, P. Ducoroy, E. Solary, Human defensins as cancer biomarkers and antitumour molecules, J. Proteome 72 (2009) 918–927.
[31] C. Melle, G. Ernst, B. Schimmel, A. Bleul, H. Thieme, R. Kaufmann, H. Mothes, U. Settmacher, U. Claussen, K.J. Halbhuber, F. Von Eggeling, Discovery and identification of alpha-defensins as low abundant, tumor-derived serum markers in colorectal cancer, Gastroenterology 129 (2005) 66–73.
[32] M. Gunes, I. Gecit, N. Pirincci, A.S. Kemik, S. Purisa, K. Ceylan, M. Aslan, Plasma human neutrophil proteins-1, -2, and -3 levels in patients with bladder cancer, J. Cancer Res. Clin. Oncol. 139 (2013) 195–199.
[33] D.A. Holterman, J.I. Diaz, P.F. Blackmore, J.W. Davis, P.F. Schellhammer, A. Corica, O.J. Semmes, A. Vlahou, Overexpression of alpha-defensin is associated with bladder cancer invasiveness, Urol. Oncol. 24 (2006) 97–108.
[34] Y. Mohri, T. Mohri, W. Wei, Y.J. Qi, A. Martin, C. Miki, M. Kusunoki, D.G. Ward, P.J. Johnson, Identification of macrophage migration inhibitory factor and human neutrophil peptides 1–3 as potential biomarkers for gastric cancer, Br. J. Cancer 101 (2009) 295–302.
[35] A. Bateman, A. Singh, S. Jothy, R. Fraser, F. Esch, S. Solomon, The levels and biologic action of the human neutrophil granule peptide HP-1 in lung tumors, Peptides 13 (1992) 133–139.
[36] C.A. Muller, J. Markovic-Lipkovski, T. Klatt, J. Gamper, G. Schwarz, H. Beck, M. Deeg, H. Kalbacher, S. Widmann, J.T. Wessels, V. Becker, G.A. Muller, T. Flad, Human alpha-defensins HNPs-1, -2, and -3 in renal cell carcinoma: influences on tumor cell proliferation, Am. J. Pathol. 160 (2002) 1311–1324.
[37] A. Lichtenstein, Mechanism of mammalian cell lysis mediated by peptide defensins. Evidence for an initial alteration of the plasma membrane, J. Clin. Invest. 88 (1991) 93–100.
[38] J. Davies, A.C. Dawkes, A.G. Haymes, R.F. Sunderland, J.C. Edwards, Scanning tunnelling microscopy and dynamic contact angle studies of the effects of partial denaturation on immunoassay solid phase antibody, J. Immunol. Methods 186 (1995) 111–123.
[39] E. Canetta, A. Riches, E. Borger, S. Herrington, K. Dholakia, A.K. Adya, Discrimination of bladder cancer cells from normal urothelial cells with high specificity and sensitivity: combined application of atomic force microscopy and modulated Raman spectroscopy, Acta Biomater. 10 (2014) 2043–2055.
[40] D. Docheva, D. Padula, M. Schieker, H. Clausen-Schaumann, Effect of collagen I and fibronectin on the adhesion, elasticity and cytoskeletal organization of prostate cancer cells, Biochem. Biophys. Res. Commun. 402 (2010) 361–366.
[41] P. Eaton, V. Zuzarte-Luis, M.M. Mota, N.C. Santos, M. Prudencio, Infection by plasmodium changes shape and stiffness of hepatic cells, Nanomedicine 8 (2012) 17–19.
[42] L.W. Francis, P.D. Lewis, D. Gonzalez, T.A. Ryder, G. Webb, L.A. Joels, J.O. White, C.J. Wright, R.S. Conlan, Progesterone induces nano-scale molecular modifications on endometrial epithelial cell surfaces, Biol. Cell. 101 (2009) 481–493.
[43] S.E. Cross, Y.S. Jin, J. Rao, J.K. Gimzewski, Nanomechanical analysis of cells from cancer patients, Nat. Nanotechnol. 2 (2007) 780–783.
[44] N.G. Papadopoulos, G.V. Dedoussis, G. Spanakos, A.D. Gritzapis, C.N. Baxevanis, M. Papamichail, An improved fluorescence assay for the determination of lymphocyte-mediated cytotoxicity using flow cytometry, J. Immunol. Methods 177 (1994) 101–111.
[45] S.T. Henriques, L. Thorstholm, Y.H. Huang, J.A. Getz, P.S. Daugherty, D.J. Craik, A novel quantitative kinase assay using bacterial surface display and flow cytometry, PLoS ONE 8 (2013) e80474.
[46] J.M. Freire, M.M. Domingues, J. Matos, M.N. Melo, A.S. Veiga, N.C. Santos, M.A.R.B. Castanho, Using zeta-potential measurements to quantify peptide partition to lipid membranes, Eur. Biophys. J. Biophys. 40 (2011) 481–487.
[47] D. Necas, P. Klapetek, Gwyddion: an open-source software for SPM data analysis, Cent. Eur. J. Phys. 10 (2012) 181–188.
[48] H.J. Butt, M. Jaschke, Calculation of thermal noise in atomic-force microscopy, Nanotechnology 6 (1995) 1–7.
[49] A. Jemal, F. Bray, M.M. Center, J. Ferlay, E. Ward, D. Forman, Global cancer statistics, CA, Cancer J. Clin. 61 (2011) 69–90.
[50] C. Morrissey, R.W. Watson, Phytoestrogens and prostate cancer, Curr. Drug Targets 4 (2003) 231–241.
[51] C. Obasaju, G.R. Hudes, Paclitaxel and docetaxel in prostate cancer, Hematol. Oncol. Clin. N. Am. 15 (2001) 525–545.
[52] T. Beer, D. Raghavan, Chemotherapy for hormone-refractory prostate cancer: Beauty is in the eye of the beholder, Prostate 45 (2000) 184–193.

[53] D.P. Petrylak, Chemotherapy for advanced hormone refractory prostate cancer, Urology 54 (1999) 30–35.
[54] J.Y. Ma, F.F. Huang, H.L. Lin, X. Wang, Isolation and purification of a peptide from *Bullacta exarata* and its impaction of apoptosis on prostate cancer cell, Mar. Drugs 11 (2013) 266–273.
[55] F. Alvarez-Calderon, M.A. Gregory, J. DeGregori, Using functional genomics to overcome therapeutic resistance in hematological malignancies, Immunol. Res. 55 (2013) 100–115.
[56] A.V. Panyutich, E.A. Panyutich, V.A. Krapivin, E.A. Baturevich, T. Ganz, Plasma defensin concentrations are elevated in patients with septicemia or bacterial-meningitis, J. Lab. Clin. Med. 122 (1993) 202–207.
[57] S. Riedl, D. Zweytick, K. Lohner, Membrane-active host defense peptides—challenges and perspectives for the development of novel anticancer drugs, Chem. Phys. Lipids 164 (2011) 766–781.
[58] Y. Zhang, M. Yang, J.H. Park, J. Singelyn, H. Ma, M.J. Sailor, E. Ruoslahti, M. Ozkan, C. Ozkan, A surface-charge study on cellular-uptake behavior of F3-peptide-conjugated iron oxide nanoparticles, Small 5 (2009) 1990–1996.
[59] I. Dobrzynska, B. Szachowicz-Petelska, S. Sulkowski, Z. Figaszewski, Changes in electric charge and phospholipids composition in human colorectal cancer cells, Mol. Cell. Biochem. 276 (2005) 113–119.
[60] D. Gaspar, A.S. Veiga, C. Sinthuvanich, J.P. Schneider, M.A. Castanho, Anticancer peptide SVS-1: efficacy precedes membrane neutralization, Biochemistry 51 (2012) 6263–6265.
[61] M.M. Ribeiro, A.R. Pinto, M.M. Domingues, I. Serrano, M. Heras, E.R. Bardaji, I. Tavares, M.A. Castanho, Chemical conjugation of the neuropeptide kyotorphin and ibuprofen enhances brain targeting and analgesia, Mol. Pharm. 8 (2011) 1929–1940.
[62] M.M.B. Ribeiro, M.M. Domingues, J.M. Freire, N.C. Santos, M.A.R.B. Castanho, Translocating the blood–brain barrier using electrostatics, Front. Cell. Neurosci. 6 (2012).
[63] I.M. Torcato, Y.H. Huang, H.G. Franquelim, D.D. Gaspar, D.J. Craik, M.A.R.B. Castanho, S.T. Henriques, The antimicrobial activity of Sub3 is dependent on membrane binding and cell-penetrating ability, ChemBioChem 14 (2013) 2013–2022.
[64] T. Iwasaki, J. Ishibashi, H. Tanaka, M. Sato, A. Asaoka, D. Taylor, M. Yamakawa, Selective cancer cell cytotoxicity of enantiomeric 9-mer peptides derived from beetle defensins depends on negatively charged phosphatidylserine on the cell surface, Peptides 30 (2009) 660–668.
[65] M.M. Ribeiro, M.M. Domingues, J.M. Freire, N.C. Santos, M.A. Castanho, Translocating the blood–brain barrier using electrostatics, Front. Cell. Neurosci. 6 (2012) 44.
[66] Y. Miyazaki, M. Aoki, Y. Yano, K. Matsuzaki, Interaction of antimicrobial peptide magainin 2 with gangliosides as a target for human cell binding, Biochemistry 51 (2012) 10229–10235.
[67] J.F. Gera, A. Lichtenstein, Human neutrophil peptide defensins induce single strand DNA breaks in target cells, Cell. Immunol. 138 (1991) 108–120.
[68] M.N. Madison, Y.Y. Kleshchenko, P.N. Nde, K.J. Simmons, M.F. Lima, F. Villalta, Human defensin alpha-1 causes *Trypanosoma cruzi* membrane pore formation and induces DNA fragmentation, which leads to trypanosome destruction, Infect. Immun. 75 (2007) 4780–4791.
[69] P.D. Antonio, M. Lasalvia, G. Perna, V. Capozzi, Scale-independent roughness value of cell membranes studied by means of AFM technique, Biochim. Biophys. Acta 1818 (2012) 3141–3148.
[70] K.S. Kim, C.H. Cho, E.K. Park, M.H. Jung, K.S. Yoon, H.K. Park, AFM-detected apoptotic changes in morphology and biophysical property caused by paclitaxel in Ishikawa and HeLa cells, PLoS ONE 7 (2012) e30066.
[71] M. Girasole, A. Cricenti, R. Generosi, G. Longo, G. Pompeo, S. Cotesta, A. Congiu-Castellano, Different membrane modifications revealed by atomic force/lateral force microscopy after doping of human pancreatic cells with Cd, Zn, or Pb, Microsc. Res. Tech. 70 (2007) 912–917.
[72] M. Girasole, G. Pompeo, A. Cricenti, A. Congiu-Castellano, F. Andreola, A. Serafino, B.H. Frazer, G. Boumis, G. Amiconi, Roughness of the plasma membrane as an independent morphological parameter to study RBCs: a quantitative atomic force microscopy investigation, Biochim. Biophys. Acta 1768 (2007) 1268–1276.
[73] M. Girasole, G. Pompeo, A. Cricenti, G. Longo, G. Boumis, A. Bellelli, S. Amiconi, The how, when, and why of the aging signals appearing on the human erythrocyte membrane: an atomic force microscopy study of surface roughness, Nanomed. Nanotechnol. Biol. Med. 6 (2010) 760–768.
[74] P. Sens, N. Gov, Force balance and membrane shedding at the red-blood-cell surface, Phys. Rev. Lett. 98 (2007).
[75] S. Suresh, Biomechanics and biophysics of cancer cells, Acta Biomater. 3 (2007) 413–438.
[76] A. Fuhrmann, J.R. Staunton, V. Nandakumar, N. Banyai, P.C.W. Davies, R. Ros, AFM stiffness nanotomography of normal, metaplastic and dysplastic human esophageal cells, Phys. Biol. 8 (2011).
[77] J. Guck, S. Schinkinger, B. Lincoln, F. Wottawah, S. Ebert, M. Romeyke, D. Lenz, H.M. Erickson, R. Ananthakrishnan, D. Mitchell, J. Kas, S. Ulvick, C. Bilby, Optical deformability as an inherent cell marker for testing malignant transformation and metastatic competence, Biophys. J. 88 (2005) 3689–3698.
[78] A.N. Ketene, E.M. Schmelz, P.C. Roberts, M. Agah, The effects of cancer progression on the viscoelasticity of ovarian cell cytoskeleton structures, Nanomedicine 8 (2012) 93–102.
[79] Z. Zhou, C. Zheng, S. Li, X. Zhou, Z. Liu, Q. He, N. Zhang, A. Ngan, B. Tang, A. Wang, AFM nanoindentation detection of the elastic modulus of tongue squamous carcinoma cells with different metastatic potentials, Nanomedicine 9 (2013) 864–874.
[80] M. Beil, A. Micoulet, G. von Wichert, S. Paschke, P. Walther, M.B. Omary, P.P. Van Veldhoven, U. Gern, E. Wolff-Hieber, J. Eggermann, J. Waltenberger, G. Adler, J. Spatz, T. Seufferlein, Sphingosylphosphorylcholine regulates keratin network architecture and visco-elastic properties of human cancer cells, Nat. Cell Biol. 5 (2003) 803–811.
[81] M.J. Hendrix, E.A. Seftor, Y.W. Chu, K.T. Trevor, R.E. Seftor, Role of intermediate filaments in migration, invasion and metastasis, Cancer Metastasis Rev. 15 (1996) 507–525.
[82] G. Zhang, M. Long, Z.Z. Wu, W.Q. Yu, Mechanical properties of hepatocellular carcinoma cells, World J. Gastroenterol. 8 (2002) 243–246.
[83] F.T. Arce, B. Meckes, S.M. Camp, J.G. Garcia, S.M. Dudek, R. Lal, Heterogeneous elastic response of human lung microvascular endothelial cells to barrier modulating stimuli, Nanomedicine 9 (2013) 875–884.
[84] L. Bastatas, D. Martinez-Marin, J. Matthews, J. Hashem, Y.J. Lee, S. Sennoune, S. Filleur, R. Martinez-Zaguilan, S. Park, AFM nano-mechanics and calcium dynamics of prostate cancer cells with distinct metastatic potential, Biochim. Biophys. Acta 1820 (2012) 1111–1120.
[85] M. Plodinec, M. Loparic, C.A. Monnier, E.C. Obermann, R. Zanetti-Dallenbach, P. Oertle, J.T. Hyotyla, U. Aebi, M. Bentires-Alj, R.Y. Lim, C.A. Schoenenberger, The nanomechanical signature of breast cancer, Nat. Nanotechnol. 7 (2012) 757–765.
[86] S. Kasas, G. Longo, G. Dietler, Mechanical properties of biological specimens explored by atomic force microscopy, J. Phys. D. Appl. Phys. 46 (2013).
[87] G. Longo, L.M. Rio, A. Trampuz, G. Dietler, A. Bizzini, S. Kasas, Antibiotic-induced modifications of the stiffness of bacterial membranes, J. Microbiol. Methods 93 (2013) 80–84.
[88] C. Roduit, G. Longo, I. Benmessaoud, A. Volterra, B. Saha, G. Dietler, S. Kasas, Stiffness tomography exploration of living and fixed macrophages, J. Mol. Recognit. 25 (2012) 241–246.
[89] M. Lekka, J. Wiltowska-Zuber, Biomedical applications of AFM, J. Biophys. 146 (2009) 012023.
[90] T.G. Kuznetsova, M.N. Starodubtseva, N.I. Yegorenkov, S.A. Chizhik, R.I. Zhdanov, Atomic force microscopy probing of cell elasticity, Micron 38 (2007) 824–833.
[91] Y.M. Efremov, M.E. Lomakina, D.V. Bagrov, P.I. Makhnovskiy, A.Y. Alexandrova, M.P. Kirpichnikov, K.V. Shaitan, Mechanical properties of fibroblasts depend on level of cancer transformation, Biochim. Biophys. Acta 1843 (2014) 1013–1019.
[92] G.Y.H. Lee, C.T. Lim, Biomechanics approaches to studying human diseases, Trends Biotechnol. 25 (2007) 111–118.
[93] Y.Y. Han, H.Y. Liu, D.J. Han, X.C. Zong, S.Q. Zhang, Y.Q. Chen, Role of glycosylation in the anticancer activity of antibacterial peptides against breast cancer cells, Biochem. Pharmacol. 86 (2013) 1254–1262.
[94] X. Meng, N.H. Riordan, H.D. Riordan, N. Mikirova, J. Jackson, M.J. Gonzalez, J.R. Miranda-Massari, E. Mora, W. Trinidad Castillo, Cell membrane fatty acid composition differs between normal and malignant cell lines, P. R. Health Sci. J. 23 (2004) 103–106.